Heat and Mass Transfer 32 (1997) 175–180

A study into CO_2 laser cutting process

B. S. Yilbas

Abstract To improve the laser cutting process, the modeling of the heating mechanism is essential. In the present study a mathematical modeling of CO_2 laser cutting process is introduced and numerical solution of the heat transfer equation is obtained. The melting front velocities at different laser output power and workpiece thicknesses are predicted. The temporal development of the melting front profile is computed. The study is extended to include the experimental study of the transient behavior of the vapor ejected from the kerf in the initial stage of the cutting process. To achieve this two methods namely He–Ne laser transmittance and fiber-optic methods are introduced. It is found that the melting front velocity is high in the early stage of the cutting process which agrees with the experimental findings.

Untersuchung des mittels CO_2-Laser erfolgenden Schneidprozesses

Zusammenfassung Zur Verbesserung des Laser-Schneideprozesses ist eine Modellvorstellung bezüglich des Aufheizmechanismus erforderlich, die in dieser Untersuchung in einer mathematischen Modellierung des CO_2-Laser-Schneidvorgangs besteht, womit numerische Lösungen der Wärmeübergangsgleichung gewonnen werden. Die Schmelzfrontgeschwindigkeit ergibt sich dabei als Funktion der Laser-Leistung und der Werkstückdicken. Auch wird die zeitliche Entwicklung der Schmelzfrontprofile berechnet. In Erweiterung der Studie erfogt die experimentelle Untersuchung des instationären Dampfaustrags an der Kerbe zu Beginn des Schneidprozesses, wobei zwei Methoden zum Einsatz kommen: He–Ne-Laser Transmittanz und faseroptische Techniken. Die rechnerisch vorausgesagte hohe Schmelzfrontgeschwindigkeit zu Beginn des Schneidprozesses wird durch den experimentellen Befund bestätigt.

1 Introduction

Laser cutting finds wide application in industry. This is mainly due to the ability of lasers to produce high quality cuts at reasonable production rates. However, there are some problems with the process that require immediate attention. The process parameters are adjusted and turned to provide the quality of cut desired, but this consumes enormous time and effort, and still the optimal cutting conditions may not be found. This is especially true when cutting different materials, in this case, whole procedure needs to be repeated.

The cutting quality deviations can be attributed to slow process drifts and disturbances. These may occur due to variation in laser cutting parameters including cutting speed, laser output power, and assisting gas pressure and optical integrity perturbations. The causes of a process producing poorer quality can be related to various interlinked reasons. In order to make many changes, the relationships between process variables and cut quality need to be investigated. Diagnosis, therefore, becomes important to improve the laser cutting quality.

The modeling of laser cutting process takes interest in the well established fields of metal treatment. Although many years have passed since the fundamentals were first developed, the theory of moving point, line, and plane sources of heat [1, 2] is a such area that receives a considerable attention in modeling of laser workpiece interaction.

In general, the cutting front is determined from the energy balance equation and simplification made for the width of the cut such that its size is the same as the diameter of the laser beam [3]. On the other hand, in laser jet assisted cutting, an attempt was made to calculate the forces exerted by an inert gas jet on the thin molten layer [4]. The dominant mechanisms governing the ejection of the melt were found to be the pressure gradient that exists within the kerf. The effect of the contribution of the chemical reaction in laser cutting process was also considered [5] and it was shown that the energy available at the workpiece surface increased up to 60% due to the occurrence of exothermic reaction. In this case, initial heating occurred through absorbed beam energy and immediately after this, the reactive gas burning started.

A laser cutting model based on a two-dimensional geometry using the Fresnel law for the absorption is introduced by Schultz et al. [6]. They developed an equation over the melting front allowing the maximum cutting depth. A model was developed by Schnocker [7] to predict the possible workpiece thickness at a known power intensity for gas assisted laser cutting. He assumed that the cutting front was vertical and covered by a molten layer. However, in reality the cutting front has inclined with an angle to the vertical direction. Consequently, to improve the laser cutting quality, the development of the realistic models become essential.

Received on 11 April 1996

Prof. Dr. B. S. Yilbas
Mechanical Engineering Department
King Fahd University of Petroleum & Minerals
Dhahran 31261
Saudi Arabia

The present study is conducted to develop a laser cutting model including the contribution of the chemical reaction due to assisting gas effect. The maximum melt front speed with laser output power and temporal variation of the melt profile are predicted. The study is extened to include experimental investigation into the detection of the initial vapor generation during the cutting process. To achieve this, transmittance of the He–Ne laser beam passing through the vapor generated on the workpiece surface is measured and the thermal radiation emitted from the vapor is detected during the initial phase of the cutting process.

2
Modelling of laser cutting

Laser cutting process may be modeled in the following manner. The laser beam considered to strikes the workpiece surface and scans it with a constant velocity, u, as shown in Fig. 1.

The workpiece is assumed to have initially a slanted edge with an inclination of 12° with respect to the laser beam direction and laser beam is assumed to interact with this inclined surface. In order to simplify the problem the workpiece width is assumed to be large as compared to its thickness and length, therefore, the governing equation of heat transfer reduces to two-dimensional form, i.e., the temperature variation in the direction of workpiece width is omitted. It is also assumed that the radiative losses from the irradiated spot is neglected. It is considered that the molten material is immediately removed at the onset of its generation and the material removal takes place only from the inclined surface of the workpiece. The spartial distribution of the laser beam across the irradiated spot is considered as a rectangular Guassian (Fig. 2). Consequently, the governing equation of heat transfer in two-dimensional cartesian coordinates is

$$\rho C_p \frac{\partial T}{\partial t} = \frac{\partial}{\partial x}\left(k\frac{\partial T}{\partial x}\right) + \frac{\partial}{\partial y}\left(k\frac{\partial T}{\partial y}\right) + q_{\text{laser}} \exp(-\delta x) \qquad (1)$$

The boundary conditions are:

At

$$t = 0$$
$$T = T_0 \quad 0 \le y \le h \quad \text{and} \quad 0 \le x \le L - y \cdot \cot g\theta$$

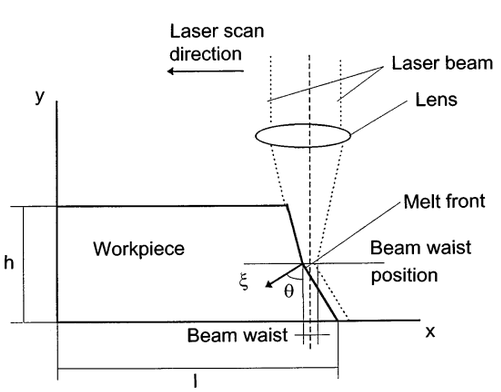

Fig. 1. A schematic view of the laser cutting front

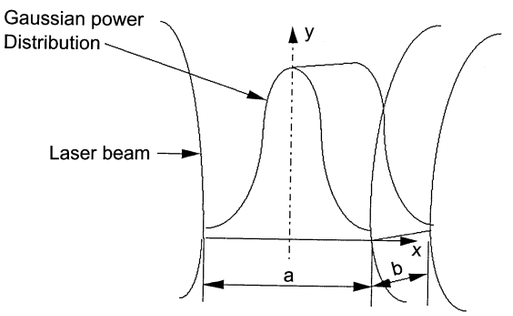

Fig. 2. Laser power intensity distribution

At

$$y = h \quad \text{and} \quad 0 \le x \le L - y \cdot \cot g\theta$$
$$\frac{\partial T}{\partial y} = -\frac{1}{k}$$

where q is the heat input.

At

$$y = 0 \quad \text{and} \quad 0 \le x \le x_{\text{melt}}(0, t)$$
$$\frac{\partial T}{\partial x} = 0 \text{ (adiabatic bottom surface)}$$

At

$$x = 0 \quad \text{and} \quad 0 \le y \le h$$
$$\frac{\partial T}{\partial x} = 0$$

At the inclined surface

$$0 \le y \le h \quad \text{and} \quad x = L - y \cot g\theta$$
$$\frac{\mathrm{d}T}{\mathrm{d}\xi} = -\frac{1}{k} q$$

However, the melt front is not known prior to melting, therefore, the above boundary condition has to be used until a melt front is established in the vicinity of the inclined edge. In the numerical solution the melt front is determined by observing the melting temperature at nodes close to the inclined surface. Once the melting temperature is reached, temperature is considered as melting temperature at any time step.

However, the heat flux per unit time should be modified to include the surface reflection. Therefore, the incident laser energy received by the workpiece at the surface becomes:

$$q_{\text{laser}} = (1 - R_f) I_0$$

where R_f is the surface reflectivity and I_0 is the laser incident power intensity.

In the case of gas assisted laser cutting process, the contribution of exothermic chemical reactions to the heat transfer taking place at the liquid surface may be written as [5]:

$$q_{\text{chem}} = \rho_e U_{H_e} C_{H_e} \Delta I \left[1 + \left(\frac{C_{H_d}}{C_{H_e}} - 1\right)\frac{h_c}{\Delta I} - \frac{B_3}{\Delta I}\right] \qquad (3)$$

where:

$$\Delta I = (I_f)_e - (I_f)_\rho + h_c \quad (4)$$

$$h_c = \sum_{i \neq E} (h_i)_g - (1+B_2)(C_i)_g] + (h_e)_g [B_2 - (1+B_2)(C_E)_g] \quad (5)$$

where B_2 and B_3 are:

$$B_2 = B_3 \frac{C_{H_c}}{C_{H_d}} \quad (6)$$

and

$$B_3 = \frac{(\rho u)_g}{\rho_e u_e C_{H_e}} \quad (7)$$

Equation (3) gives the heat transfer to the liquid metal due to chemical reactions and mass transfer receiving at the assisted gas–liquid interface when a reacting turbulent layer flows over the liquid molten metal. Therefore, the total heat flux available at the surface becomes:

$$q = q_{\text{laser}} + q_{\text{chem}} \quad (8)$$

The distribution of energy flux due to incident laser beam is considered as a rectangular Gaussian type Fig. 2, i.e.,

$$q_{\text{laser}} = -\frac{2I_0 \exp(-4x/a)^2}{\sqrt{\pi} \cdot a \cdot b} \quad (9)$$

where

$$a = a_0 + \frac{(c - a_0) \cdot |y - h/2|}{f}$$

3 The material removal

The rate of material removal and the melting front velocity may be calculated in the following manner. Once the temperature reaches to the melting temperature, Stefan boundary condition for the continuity of heat flux should be used to determine the melt front velocity and subsequently the location of melt front at advanced time step may be determined from:

$$\rho L V = \frac{2w \exp[-(4x/a)^2]}{\sqrt{2\pi} \cdot ab} \cdot \sin\beta + k \frac{\partial T}{\partial \xi} \quad (10)$$

at

$$x = x_{\text{melt}}(y, t) \quad \text{and} \quad 0 \leq y \leq h$$

where V is the melt front velocity at any point on the melt surface in a direction perpendicular to the surface at that point. The location of melt front at an advanced time step is found from its displacement given as:

$$\Delta\xi = V \cdot \Delta t \quad (11)$$

The rate of material per unit width of the workpiece may be determined from:

$$\dot{m} = \int V \, ds \quad (12)$$

where ds is the incremental length along the melt front and V is the melting front velocity to be determined from Eq. (10). However, the average propagation velocity of the melting front in the direction of the workpiece movement may be written as:

$$V_x = \frac{\dot{m}}{A_{\text{projected}}} \quad (13)$$

where $A_{\text{projected}}$ is the projected area per unit width in the plane perpendicular to the workpiece movement.

To solve the governing equation (Eq. (1)) a numerical scheme using a finite difference method was used, i.e., explicit scheme was introduced to descritized the Eq. (1), which in turn the temperature field at the advanced time domain was predicted. The time increment δt was selected according with the stability criteria. The material properties were considered as polynomial function of temperature, therefore, the constants of these polynomial equations were taken from the existing data available for the steel [9]. The mass removal rate and the velocity component in the direction of workpiece motion were determined numerically using a Simpson rule.

4 Experimental

A CO_2 laser delivering nominal output power of 850 W was used to irradiate the target. A ZnSe lens of 10 mm focal length was used to focus the laser beam on the workpiece. A convergent nozzle allowing assisting gas purging coaxially with the laser beam was employed, and noting that the nozzle exit diameter was about 0.8 mm, which provided no chopping effect of the laser beam.

In order to monitor the vapor ejection during the initial part of the cutting process, two techniques were employed. These include He–Ne laser transmittance due to vapor ejection and fiber-optic detection technique for the thermal radiation emitted from the vapor ejected (Fig. 3). In the first technique, the He–Ne laser beam first passed through the section under examination until it reached one of the photo detectors. This resulted in a shift in photo detector output. However, to observe the vapor absorption during CO_2 laser cutting process, the photodiode outputs were initially set to coincide. Once the cutting started, plasma developed and both photodiodes gave responses, one due to thermal radiation emitted from the vapor ejected and the other due to thermal radiation and the

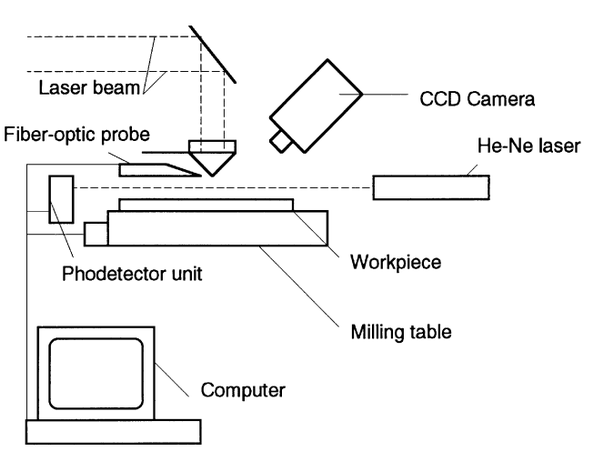

Fig. 3. Experimental set up

He–Ne laser beam, resulting in a shift in direction opposite to the gain of the photodetector outputs. This appeared as a gap between two signals on the oscilloscope. Since the initial shift due to the He–Ne laser beam was known, the transmittance (I/I_0) could be determined from the oscilloscope outputs. The deviation of detector output signals due to the thermal radiation was taken into account through switching off the He–Ne laser before firing the CO_2 laser. The output of detectors is shown in Fig. 4.

To monitor the size of the vapor emitted from the workpiece the thermal radiation emitted from the vapor was monitored using a fiber-optic probe. The fiber-optic probe consisted of 1.5 mm long and 0.8 mm diameter fiber cable and fast response photodiode. The photodiode was situated at the one end of the fiber cable. The fiber cable was positioned 10 mm away from the workpiece surface and 15 mm away from the CO_2 laser beam axis (Fig. 3). This provided clear view of the irradiated spot by the fiber-optic probe. The probe output is shown in (Fig. 5).

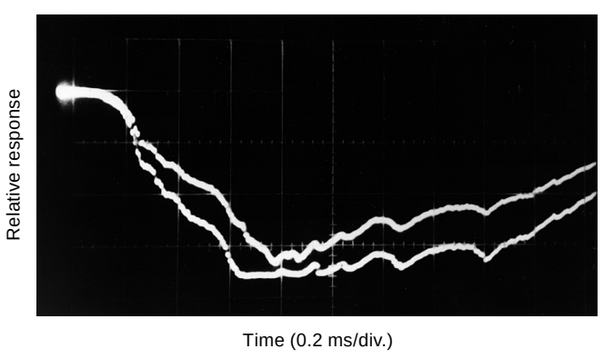

Fig. 4. Detectors output for He–Ne laser transmittance test

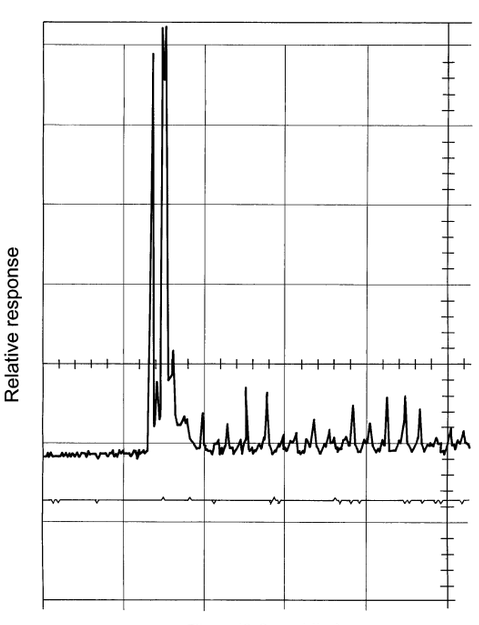

Fig. 5. Fiber-optic probe output

5 Discussions

The temporal variation of melting front velocity is shown in Fig. 6 as the laser scan speed is variable. In the early phase of the cutting process, the melting front velocity is relatively high and it reduces to almost steady value as the cutting progresses. This is due to that the peak power intensity of the laser beam falls on the melt surface in the initial part of the cutting process, which in turn results in higher temperature rise in this region. In this case the rate of melting is high and as a consequence of this the melting point attains higher velocity than the laser scan velocity. Consequently, as the cutting progresses, the melt front recedes away from the laser axis due to its high speed, resulting in less laser power reaching this region, therefore, considerable reduction in the melt front velocity occurs. When the value of the melt front velocity approaches to that of the laser beam, the moving melt front stays almost a fixed distance away from the larger axis, i.e., the heat flux received by the workpiece remains about constant which in turn results almost constant temperature gradient after the initial transient period. On the other hand, when setting the value of laser scan speed same as the initial value of the melting front velocity, almost constant melting front velocity is resulted. It should be noted that if the laser scan velocity increases beyond this value, the cutting ceases, i.e., the maximum attainable cutting speed is, therefore, considered as equal to a melting front velocity.

Figure 7 shows the temporal variation of melting front velocity with the workpiece thicknesses. The general trend of the melting front velocity is the same as indicated in Fig. 6. Increasing thickness results in relatively low melting front velocities. However, this difference is quite small. This may be closely related to the temperature gradient at the melting zone, in this case, the conduction losses occurring for thicker workpiece is higher than that corresponds to the thinner workpiece. It should be noted that the recoil pressure developed in the kerf is not taken into account in the calculations, therefore, momentum effect due to recoil pressure has no influence on the mass removal rate.

Figure 8 shows the temporal variation of melting front velocity for different laser output power intensities. The

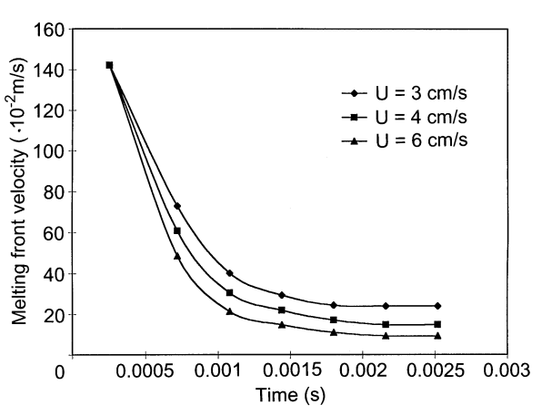

Fig. 6. Temporal variation of melting front velocity, obtained at 400 W laser output power, for different laser scanning velocities and 0.8 mm thick workpieces

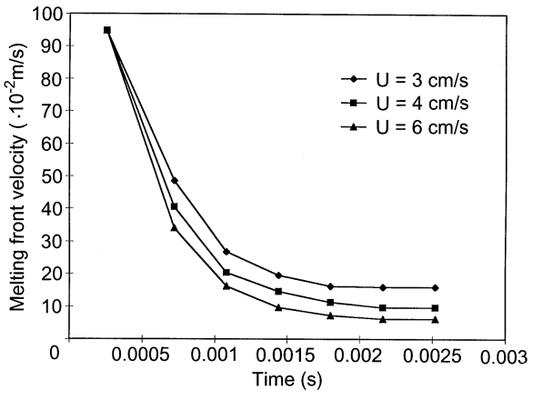

Fig. 7. Temporal variation of melting front velocity, obtained at 400 W laser output power, for different laser scanning velocities and 1.2 mm thick workpieces

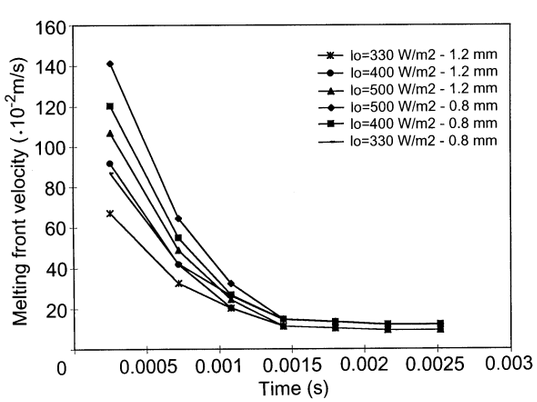

Fig. 8

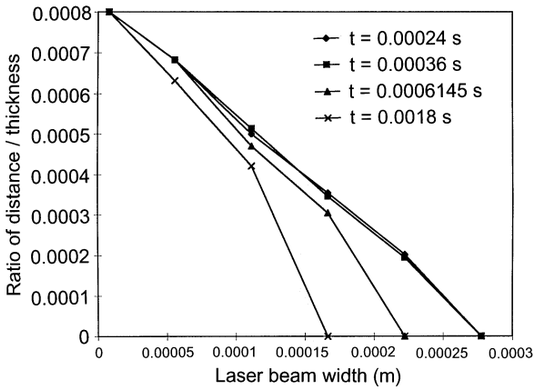

Fig. 9

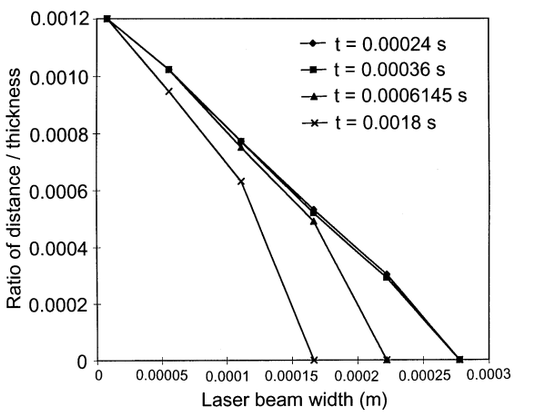

Fig. 10

melting front velocity increases with increasing laser power intensity in the initial stage of the cutting process. However, as the cutting progresses, the melting front velocity approaches to steady state value. This is true for a given thickness. On the other hand, as the thickness increases, the melting front velocity slightly reduces. It is evident that for a known workpiece thickness, the melting front velocity is a function of the laser output power.

Figures 9 and 10 show the melting front profiles for different workpiece thicknesses. The melt front profile reaches the steady state profile after a short time from the start of the cutting processes. In the initial phase of the cutting process the melt front geometry varies with time and the steady state profile appears to be in almost a sharp front edge providing that some inclination (12°) occurs from the upper surface to the 40% of the workpiece thickness. This part is almost the same for the other cases as it is seen in the initial phase of the cutting process. The melting front profile remains vertical beyond 40% of the thickness to the bottom surface of the workpiece. The influence of laser output power on the steady state melting front profile seems to be less significant.

In connection with the transmittance test results (Fig. (1)), in the very early initiation of the cutting process, the vapor ejection from the workpiece surface is low, but reaches to almost maximum after a few ms. This may be due to that laser incident power available in this region is high, since the laser power has not moved some distance away, and the pressure developed in the cavity is also high resulting in high rate of vapor ejection. However, as the penetration of the workpiece is progressing, the beam moves some distance away from the initial point, due to the scanning speed of laser, the power available at the initially irradiated point drops, therefore, the rate of vapor ejection reduces, which in turn increases the transmittance of the He–Ne beam. This also agrees well with the theoretical prediction, i.e., the melting front velocity is higher resulting in high mass removal rate in the early stage interaction process. As the laser power intensity increases the increase of transmittance with time reduces (Fig. 4). This may again be explained in terms of the laser power available at the initially irradiated point where the measurement is referenced. Therefore, the power available at this point is higher than that corresponds to low laser power, in this case, the mass removal

rate is expected to be higher, which in turn gives less transmittance of He–Ne laser beam. This agrees will with the theoretical predictions, i.e., increasing laser power intensity results in increased melting front velocity, which in turn increases the mass removal rate.

The fiber-optic probe response is higher at the initial stage of the cutting and decreases as the cutting progresses (Fig. 5). This indicates that the thermal radiation emitted from the vapor reference to heated spot is considerably high in the initial stage of the cutting process indicating the high rate of mass removal. It should be noted that as the vapor ejection increases so the removal rate increases, in this case, the thermal radiation emitted from the vapor on the workpiece surface increases. As the laser scans further, the power available at this point drops resulting in less melting front velocity developed as discussed before. This, therefore, agrees well with the results obtained from the transmittance test and the theory. It is also evident that some variation in probe response with time occurs. This may be due to the coupling effect of the vapor heating and vapor absorption of incident laser beam, which was predicted in the previous study [10], i.e., once the size of the vapor increases, it absorbs the incident laser energy and as a result the temperature and pressure of the vapor increases. This vapor then expands rapidly, which in turn produces less vapor on the workpiece surface.

6 Conclusions

The melting front velocity is considerably high in the early stages of the cutting process. As the cutting progresses, it attains a steady state value, in this case, the moving melt front appears almost a fixed distance away from the laser axis. Therefore, the heat flux due to incident laser beam, received by the workpiece remains almost constant. As the cutting velocity increases so the melting front velocity approaches to the laser scanning velocity and beyond this value the cutting ceases. As the workpiece thickness increases the melting front velocity reduces. This may be due to the conduction losses related to the workpiece thickness. However, the melting front velocity increases with increasing laser output power and it is evident that the melting front velocity is the function of laser output power and workpiece thickness.

The steady state melting front profile is attained just after the initiation of cutting process. In the initial part of the cutting process, the melting front profile remains almost vertical beyond 40% of the workpiece thickness to the bottom surface. Once the steady state melting front is established, the laser output power has almost no influence on the melting front profile.

The transmittance test results prevail that in the early stages of the cutting process, the vapor ejection is high resulting in high mass removal rate, this may suggest the occurrance of the high melting front velocities. This result agrees well with the theoretical predictions. On the other hand, fiber-optic results indicate the similar finding that is observed from the transmittance test. The detection of thermal radiation from the vapor ejected indicates that the vapor ejection may occur in a cyclic form.

References

1. **Olsen, F.O.:** Cutting front formation in laser cutting. CIRP, 38(1) (1989) 215–218
2. **Akhter, R.; Davis, M.; Dowden, J.; Kapadia, P.; Ley, M.; Steen, W.M.:** A point and line source model for laser keyhole welding. J. Phys. D 21 (1988) 1255–1260
3. **Yilbas, B.S.; Davies, R.; Yilbas, Z.:** Study into measurement and prediction of penetration time during CO_2 laser cutting process. Proceedings of Instn. Mech. Engrs., Part B: J. Engineering Manufacture 204 (1990) 105–113
4. **Yilbas, B.S.; Davies, R.; Yilbas, Z.:** Investigation into development of liquid layer and formation of surface plasma during CO_2 laser cutting process. Instn. Mech. Engrs., Part B: J. Engineering Manufacture. 206 (1992) 287–298
5. **Yilbas, B.S.; Sahin, A.:** Turbulent boundary layer approach allowing chemical reactions for CO_2 laser-assisted cutting process. Proc. Instn. Mech. Engrs., Part C: J. Mechanical Engineering Science 208 (1994) 275–284
6. **Schultz, W.; Becker, D.; Franke, J.; Kemmerling, R.; Herziger, G.:** Heat conduction losses in laser cutting of metals. J. Phys. D 26 (1993) 1357–1363
7. **Schnocker, D.:** Theoretical model of reactive gas assisted laser cutting including dynamic effects. SPIE Proc. 650 (1986) 210–219
8. **DeHoff, R.T.:** Thermodynamics in Materials Science, McGraw-Hill, New York, 1993
9. **Duley, W.W.:** Laser Processing and Analysis of Materials. Plenum Press, New York, 1983
10. **Yilbas, B.S.; Davies, R.; Yilbas, Z.:** Study into measurements and prediction of penetration time during CO_2 laser cutting process. Proceedings of Instn. Mech. Engrs. Part B: J. Engineering Manufacture 204 (1990) 105–113